

# Physically Interpretable Diffractive Optical Networks

Ruitao Wu,<sup>†</sup> Juncheng Fang,<sup>†</sup> Rui Pan, Rongyi Lin, Kaiyuan Li, Ting Lei,<sup>\*</sup>  
Luping Du,<sup>\*</sup> and Xiaocong Yuan<sup>\*</sup>

*Nanophotonics Research Centre, Institute of Microscale Optoelectronics & State  
Key Laboratory of Radio Frequency Heterogeneous Integration, Shenzhen  
University, Shenzhen 518060, China.*

<sup>\*</sup> Corresponding authors: [leiting@szu.edu.cn](mailto:leiting@szu.edu.cn), [lpdu@szu.edu.cn](mailto:lpdu@szu.edu.cn),  
[xcyuan@szu.edu.cn](mailto:xcyuan@szu.edu.cn)

<sup>†</sup> These authors contributed equally to this work.

## Abstract:

Inspired by neural network algorithms in deep learning, diffractive optical networks have arisen as new platforms for manipulating light-matter interactions. Inherited from the deep learning black box nature, clear physical meanings have never been given for these complex diffractive networks at the layer level, even though the systems are visible in physical space. Using exemplified mode conversion systems, we show how various physical transformation rules within diffractive networks can be unveiled given properly defined input/output mode relations. Surprising physical transformation division phenomenon and an optical analogy of gradient-vanishing-effect have been observed and discussed for high-dimensional mode sorting tasks. The use of physical interpretation for efficiently designing a parameter-varying network has also been demonstrated. These physically interpretable optical networks resolve the contradiction between rigorous physical theorem and operationally vague network structure, and pave the way for further interpret advanced deep learning tasks and other physical neural networks.

## Introduction

Being one of the most successful machine learning approaches, deep learning (DL) has achieved remarkable performance in a variety of practical tasks, including image classification, speech recognition, bioinformatics, optical microscopy, and many more<sup>1</sup>. Inspired by the widely used neural networks (NNs) structure in DL, diffractive networks (DNs) have been proposed and demonstrated to perform optical computing at the speed of light in a power-efficient manner<sup>2,3</sup>. The superior processing capability, flexibility, and robustness of DN originate from their complex network architectures, even when the system is designed solely for linear transformation of input optical waves<sup>4-6</sup>. However, despite all the advancements, challenges remain in understanding and interpreting the operations behind these complex networks.

One of the most critical challenges in DL and its optical counterpart, DN, is model interpretability, which is often referred to as the ‘black box’ nature of these systems<sup>7</sup>. In DL, it is difficult to understand the exact operations behind a trained NN, as exemplified by the convolutional neural networks (CNNs) shown in Figure 1a. The inability to interpret models has led to confusion and lack of confidence, sometimes can even cause ethical and legal concerns<sup>8,9</sup>. Due to the shared network complexity, optical DN inevitably inherit these issues. Ironically, even though trained DN are implemented in physical systems that are fully visible to both the designers and users, the mathematical meanings behind them remain vague and elusive.

Contrary to the extensive efforts devoted to interpreting NNs in DL<sup>10,11</sup>, investigation into the mathematical operations underlying DN has been quite limited. To our knowledge, while seemingly meaningful patterns have appeared in several reports, clear physical interpretations at individual layers of reported models have never been discussed or provided<sup>2,12,13</sup>. With the rapid development of DN and other optically implemented NNs across diverse problems and disciplines, it becomes critical to tackle this issue. Physically interpretable DN are expected to be both intuitive and generalizable, which could bring new insights for further research on systems akin to artificial neural networks (ANNs)<sup>14-16</sup>.

Here, we present physically interpretable diffractive optical networks (Fig. 1b), in which the meaning of each layer within the DN is unveiled. The exemplified networks are built upon mode conversion tasks using cascaded diffractive surfaces, where mode indices of the input structured beams are identified and classified<sup>17</sup>. We demonstrated how various physical transformation rules can emerge from initially void layers after training the DN with specific input-output mode relations and dimensionalities. For high-dimensional mode conversion DN, an intriguing physical transformation division phenomenon appears, accompanied with our first observation of an optical analogy of gradient-vanishing-effect in DL. Furthermore, we demonstrate how such physical interpretation helps to reduce the computational effort when designing high-performance, high-dimensional DN in the presence of system variations. Our study has not only provided new methods for understanding and designing DN, but also has significant implications for other research based on network configurations.

## Results

### Re-discovery of coordinate transformation rules within diffractive networks

We illustrated our concept by training DN as classifiers for optical modes according to their mode indices. Such a classification process is also known as mode demultiplexing/sorting in the optical community. Essentially, the computation procedure can be thought of as a mode conversion process, as any linear device, such as diffractive layers in DN, has been proven to be physically equivalent<sup>18,19</sup>. Theoretically, it can be considered as a conversion of Hilbert space from mode index spectrum to spatial distribution<sup>20</sup>. We will show how conventional mode conversion rules emerge for these trained complex networks with different layers. In this paper, we will focus on the demultiplexing of the Laguerre-Gaussian (LG) modes<sup>21</sup>, which are described by two quantized indices,  $l$ , the topological charge, and  $p$ , the radial number (Supplementary Note 1). The possibility of using other optical modes and generic inputs (such as images) will be given later in the discussion section.

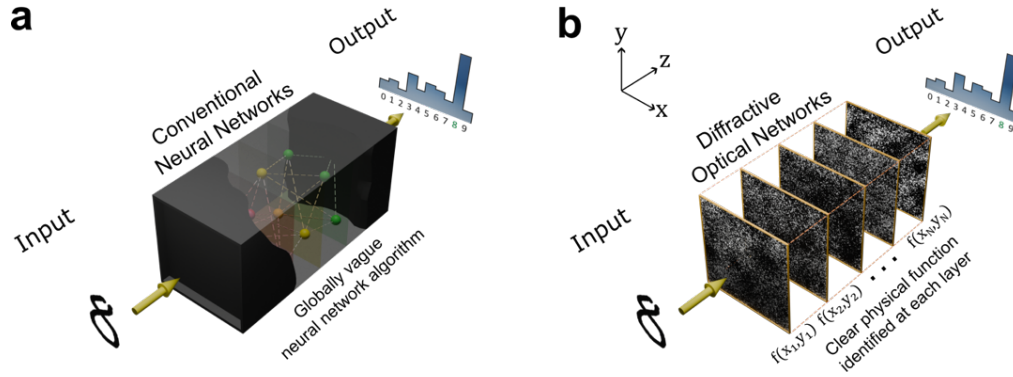


**Fig. 1. Concept of the physically interpretable diffractive optical networks.** (a) Conventional neural network. The algorithm is typically considered a global “black box” since it gives the output in a way that is not physically intuitive and understandable for each layer. (b) Diffractive optical network implemented on physical space to conduct optical computing. The physical meaning of this optical analogy neural network remains unclear, mainly due to the seemingly random phase masks and complex intra-layer connections. This work will show how to interpret such networks and unveil their physical meaning per layer level.

We first consider a two-layer diffractive structure that can perform input LG mode sorting according to their orbital angular momentums (OAMs) (Fig. 2a)<sup>22</sup>. We will only consider the case of  $p=0$ , meaning they are vortex beams carrying OAMs of integer numbers. The case when  $p \neq 0$  will be discussed in the next section. The outputs are set to be Gaussian-like modes distributed along the x-axis. Our dataset consists of 11 LG modes with  $l$  from -5 to 5, while  $l = 4, 2,$  and  $-2$  are randomly picked to be the test set, and the rest are used as the training dataset. More detailed information is provided in Materials and Methods. We will soon show how these two diffractive layers can work synergically to perform coordinate transformation as an afocal system and then perform the mode sorting task.

The trained masks are presented in Fig. 2b (top line), where an interesting continuous phase gradient can be observed within the region of interest (ROI), enclosed by the red dotted lines, where most of the energy is distributed. The trained network is physically implemented on a multi-plane light conversion system, with details provided in Materials and Methods. The network performance is characterized by a detection probability matrix (Fig. 2c), with an average of 77% (numerically) and 72% (experimentally).

What is interesting is that the shapes of ROIs transform from a circle to a rectangle for two different masks, respectively. This reminds us about a critical functionality of diffractive surfaces, i.e., performing coordinate transformation<sup>23</sup>. In fact, the task which the DN is trained for is vortex mode sorting, a typical problem in the field of optics. One of the elegant solutions is to apply the log-polar transformation, and then use a lens to focus the transformed field in the output plane. This task requires a minimum of two masks<sup>24</sup>. The first mask acts as a log-polar transformation unwrapper, and the second mask performs the phase correction and the focusing (Fig. 2a). We noted that transformation terms within these two masks strongly depend on each other since they form an afocal system together<sup>25</sup>. The exact parameters of both masks, however, can be retrieved from the trained network and calculated analytically, as detailed in Supplementary Note 2.

Masks of analytical solution for the log-polar transformation method are shown in Fig. 2b (bottom line). Surprisingly, the trained DN resembles the coordinate transformation theory very well within the ROIs, since these are where the energy is distributed. We further extracted the transformation term within these two mask pairs and verified that the functionality of our trained network performs the same as the aforementioned theoretical approach, as numerically evaluated and experimentally verified in Fig. 2d.

Overall, we have shown how our trained DN learned about the well-known “log-polar transformation and focusing” approach after training for a vortex mode sorting task. The functionalities of all layers are unveiled, and the resultant trained network matches the theoretical prediction well. Other types of operations, such as circular-sector transformation and beam shaping,

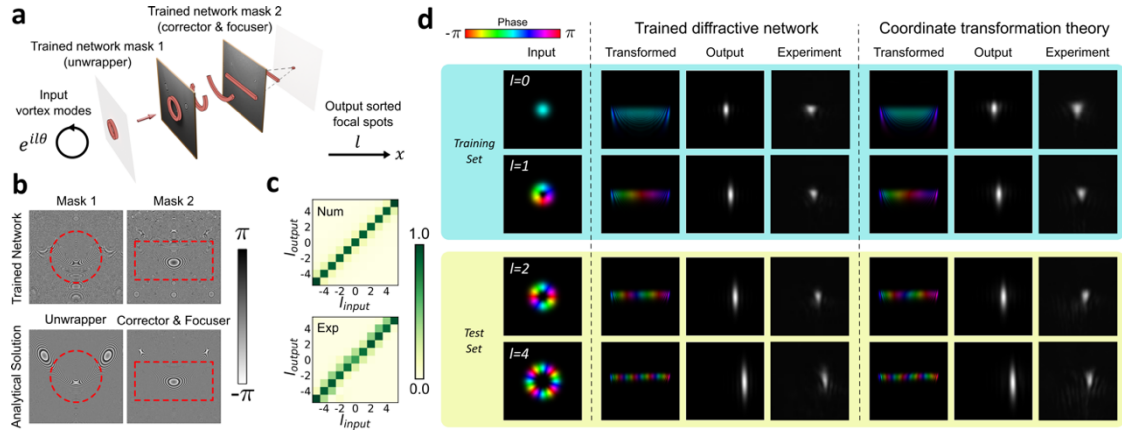


**Fig. 2. Physically interpretable diffractive network as a vortex mode sorter: re-discovery of the log-polar transformation approach.** (a) Sketch of a two-layer DN for vortex mode sorter. (b) The trained mask pairs resemble the log-polar transformation, while one mask acts as the unwrapper and the other one serves as the corrector and the focuser. Red dotted lines indicate the region of interest, where optical power is focused. (c) The detection efficiency matrix for the trained network as a mode sorter. (d) Verification of the transformation process for both the log-polar mode sorter and the trained network. The images show the phase of numerical model light fields (colorful images) and the intensity (grayscale images, both numerical and experimental data). Noted that the intensity images are magnified by 4 times with respect to the field images.

can be realized with such a system, once a proper relation between the input/output mode is defined, which is demonstrated in the following.

### Unveiling physics within diffractive networks for high dimensional mode sorting

Next, we show how different physical processes can separate from each other for a trained network of high dimensionality. We move on to a mode converter that can simultaneously sort both indices of input LG modes into a 2D rectangle distribution. The dimensionality of the DN is increased by incorporating the radial index and assigning it to the y-axis, while the index  $l$  is distributed into the orthogonal x-axis. Although the design of a seven-layer diffractive LG mode sorter has been experimentally demonstrated, the functionality of each diffractive layer within the diffractive network remains unclear<sup>17</sup>. Intuitively, one would expect a minimum of three layers since we would need at least one more mask to deal with factor  $p$ . Therefore, in this section, we consider a DN with three diffractive layers. The details about the training can be found in Materials and Methods.

The physical transformation within the trained network is sketched in Fig. 3a. Aside from the focuser in the last plane, two distinct diffractive processes can be identified after computing the input fields with forward propagation. First, a diffractive process that performs the circular-sector transformations<sup>26</sup>, resulting in sector-shape output fields carrying azimuthal phase gradients<sup>24</sup>. We noted that such transformation is slightly different from the reported works since it involves a term that performs center positioning. Second, the multiple sectors (depending on  $p$  values) will be reshaped into a relatively uniform circular distribution with a phase gradient along y-axis, which can lead to repositioning after focusing. We noted that there are no rigorous analytical solutions for such a process, as the radial factor  $p$  has proved to be challenging to sort using diffractive elements<sup>27</sup>, which leads to discontinuity in mask 2. Nevertheless, these two physical processes are identified and their corresponding terms can be obtained separately (the second one is calculated using an interactive phase-matching algorithm<sup>28</sup> and given for comparison), as shown in Fig. 3b. Details about the phase terms retrieval within the trained DN are given in Supplementary Note 3.

The physical functionality of each layer for the trained DN becomes clear, as summarized in Fig. 3d. The crosstalk matrices and the final output fields for the trained network are also numerically calculated and experimentally verified in Fig. 3c. Good agreement with the theoretical physical transformation is found. We demonstrated that such a high dimensional mode conversion task can be realized by increasing the number of diffractive layers. In contrast, each layer has its own distinct physical meaning. Additionally, what is interesting about this network, as compared to the previous one, is that rigorous coordinate transformation solutions can be found in both cases, which is

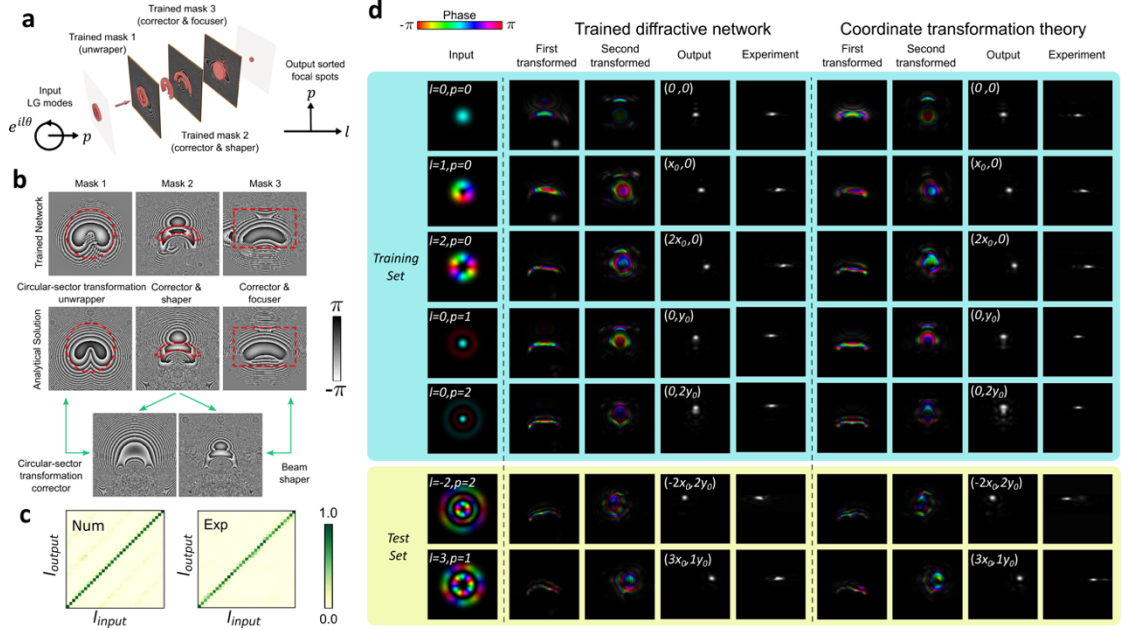


**Fig. 3. Physical interpretable triple-layer LG mode converter: independence of multiple physical transformations.** (a) Sketch of the trained triple-layer DN for LG mode sorter, where the index  $l$  is sorted along the x-axis and the  $p$  value is distributed to the y-axis. (b) The LG mode sorting process in LG modes involves two transformations: 1. Circular-sector transformation. 2. A beam shaper turns the sector to a disk distribution with varying phase terms, as well as a radial lens that performs the focusing. Red dotted lines indicate the regime where optical power is focused on. (c) The detection efficiency matrix for the trained network as a LG mode sorter. (d) Verification of the transformation process for both the LG mode sorter and the trained network. The images show the phase of numerical model light fields (colorful images) and the intensity (grayscale images, both numerical and experimental data). Noted that the intensity images are magnified by 4 times with respect to the field images.

unknown knowledge for the network before the training. The trained network extracts this information, making the sorting of the test set to be easily understood.

### Physical transformation division within complex diffractive networks

Similar to the choice of network layers in DL, when designing such a network, the diffractive surface numbers in DNs seem uncritical compared to other many other parameters. However, it does have several constraints in physical aspects. Intuitively, small diffractive surfaces cannot convert complex modes with high purities<sup>17</sup>. On the other extreme, the alignment of a large number of masks can be technically challenging, not to mention the external environmental conditions like mechanical vibrations, or input scaling and rotations<sup>5</sup>. To our knowledge, there has not yet been any study on the effect of surface numbers within DNs. Here we investigate the evolution of all the physical processes when designing a DN.

We follow the discussion of our two-dimensional LG mode classifier and extend it to the case of various numbers of diffractive masks (denoted by  $N$ , from 2 to 7). The trained DN and relevant results are summarized in Fig. 4. We noted that the phase correction functions are omitted for illustration purposes. Details regarding the training can be found in Materials and Methods. Analysis of physical transformation in each mask is given in Supplementary Note 4.

An intriguing phenomenon appears when checking the evolution of physical processes for each mask within Fig. 4. For a small number of layers, such as  $N \leq 2$ , as expected, no physical solutions are available for the LG mode conversion task. For  $N=3$ , we recover a similar example in the previous section, where a circular-sector transformation and a diffractor that can simultaneously reshape and reposition the beam are observed. When  $N$  is increased from 3 to 7, one can observe a “physical transformation division” process: the functionality of one diffractive mask for a DN of  $N$  layers will be performed by two consequent surfaces for DN of  $N+1$  layers, as indicated by red arrows. For instance, when  $N$  increases from 4 to 5, the log-polar transformation is divided into two: a circular-to-sector transformation and a sector-to-cartesian transformation. Surprisingly, it has been

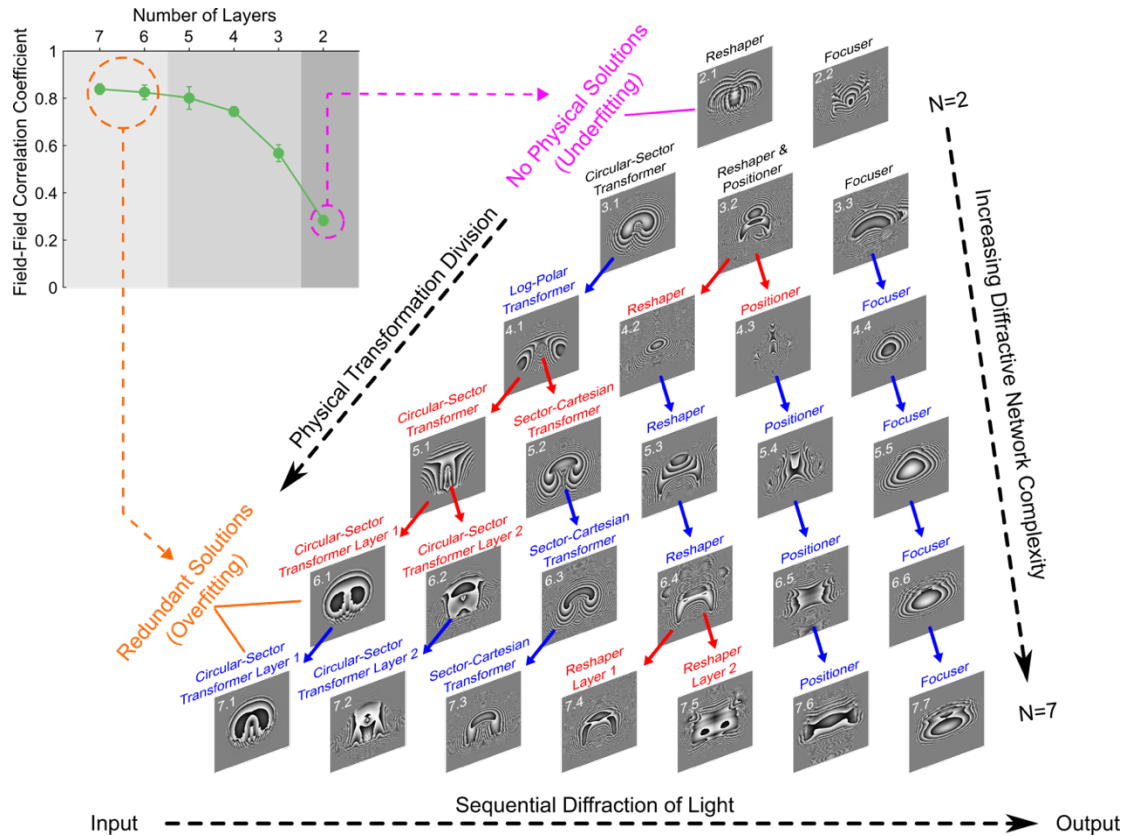


**Fig. 4. Physical transformation division phenomenon in multi-layer diffractive networks trained for LG mode classification.** When training a diffractive network for a specific mode classification task, with increasing network complexity (number of layers), the functionality of each diffractive mask can either be maintained (blue arrows) or split into two sequential layers (red arrows). The top left inset image shows the correlation coefficient between the designed and numerical output field, as a function of diffractive surface numbers. Error bars indicate the standard deviation of correlation coefficients over all the input modes. Such a physical transformation division process can range from very few layers when there are no known physical solutions (underfitting, with an extremely low correlation coefficient), to multiple-layer cases in which redundant mask solutions appear (overfitting). In the intermediate regime (mask number from 3 to 5), clear physical transformation processes can be identified for each layer, while the system performance increases significantly. In the case of overfitting, the performance of the system does not benefit from the increasing number of masks since the correlation coefficient remains unchanged. Noted that every mask in each system (except from the first mask), also performs a phase correction function, which is omitted for simplicity.

demonstrated that a polar to cartesian transformation can only be done with at least three surfaces<sup>23</sup> (that is why log-polar is used instead of polar for vortex mode sorting). Such knowledge is captured by the designed DNs. Starting from  $N=6$ , a “physically redundant” mask appears, as now a circular-sector transformation will require three masks instead of two (Mask 6.1 and 6.2). We attributed this interesting phenomenon to the physical transformation division effect, which is analogous to the gradient vanish effect in CNN<sup>29</sup>. The redundancy of these masks can be further verified by calculating the field-field correlation coefficient of the targeted field and the numerically evaluated output field, as now this parameter saturates after  $N \geq 6$ . Surprising correlation between the field-field correlation coefficient and appearing of the redundant solutions has been found, indicating the gradient-vanish feature of such network, since the additional hidden layers of the system does not improve the system performance. We noted that the field-field correlation coefficient is a strict quantity compared to the detection matrix since it requires not only the integrated intensity but also the local amplitude and phase distributions. Lastly, some masks perform identical functions for different systems, and their sequences within the network remain the same. A good example is the focuser, which always appears as the last surface, as the exemplified network is trained as a sorter with performance evaluated by integrated spots. This lensing effect in the last mask can also be found in other literatures<sup>2</sup>.

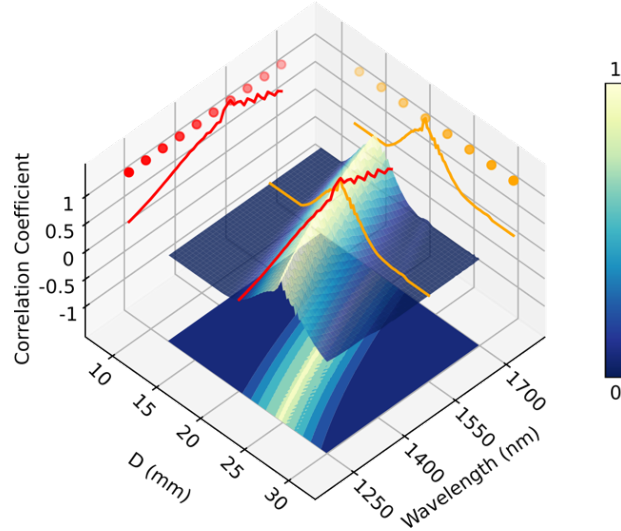


**Fig. 5. Extrapolation of a physical interpretable diffractive network under system variations.** For the system proposed for vortex mode sorting optimized for single wavelength (1550 nm) and interplane distance (20 mm), the correlation coefficient of designed sorted spots and numerically output fields will severely degrade under system perturbation (see contour). The re-training of new networks takes effort and time. However, since the network has “learned” about the coordinate transformation behind, the “analytical” solution can be extended to other wavelengths (red dots) or distances (yellow dots) with almost unity correlation coefficients.

### Application of physical interpretation

We devoted the last section to applying the obtained physical interpretation for designing new DNs with system variations. We will still consider the aforementioned two-layer system designed for vortex beam sorting as an example. Typically, a trained DN needs to be re-trained when the system parameter(s) changes. However, since the trained DN is found to be an optical system that performs log-polar transformation, we can apply the intrinsic property of coordinate transformation and extend such a network with system variations. We would like to emphasize that such extrapolation does not require the knowledge of analytical solutions for the transformation or extraction of model parameters. Details of the extrapolation can be found in Supplementary Note 5.

We considered the extrapolation of previously trained DN to other wavelengths and interplane distances. Results are summarized in Fig. 5. While there is a limited bandwidth for both wavelength (red curve) and distance (yellow curve), it is possible to extrapolate the trained network and directly calculate the new mask without performing new training<sup>30</sup>. The performance of the new masks will have an identical performance to the original masks.

### Discussion

Diffractive optical networks have been a powerful platform for performing deep learning algorithms at the speed of light. There has been plenty of research on the mathematical limitations of these networks<sup>4,31</sup>. However, to our knowledge, there have been no attempts to interpret the physics behind the seemingly complex multi-layer diffractive layer structure. A good starting point is to build up a relation between the input and output modes since the linear operation is theoretically equivalent to mode conversion<sup>18</sup>. In this work, we started with a simple vortex mode sorting example and showed how the conventional vague DN can be turned into an interpretable diffractive network through forwardly propagating the input modes and analyzing the intermediate mode states. Surprisingly, our two-layer DN rediscovers the famous log-polar transformation and focusing procedure for vortex mode sorting. Following this example, we later demonstrated how such physical interpretation can be used to extrapolate the trained network under physical perturbations and eliminate the need for re-training. These results theoretically connect the seemingly complex diffractive layers and conventional diffractive rules in Fourier optics<sup>32</sup>.

Another problem we tackled is the collective physical phenomenon behind multiple diffractive layers. We first demonstrated that the increase of classification dimensionality can be incorporated

with the additional network layer, while maintaining the independence of both physical processes, respectively. While previous research focused on capacity limits, we take a distinct perspective by looking at the number and evolution of transformations within a DN with varying layer numbers. We have also discovered an intriguing physical transformation division phenomenon when the diffractive layer of the network increases and reported the first observation of physically redundant solutions in DNs when two sequential diffractive layers work synergically to achieve only one transformation. This effect is akin to the gradient-vanishing-effect in DL, where one or more neural layers have little influence on the final outputs. To our knowledge, this effect is the first observation of gradient-vanishing-like effects in DNs. Such a division process has increased the understanding of collective effects within the system and will help to design high-performance, high-dimensional diffractive optical networks compactly and robustly.

We have chosen to present our work with examples within the mode conversion framework and used LG modes as examples. Essentially, any input two-dimensional complex field can be decomposed into a linear superposition of any orthogonal modes that form a completed set. Thus, the understanding of the conversion of these modes within these complex networks will certainly be critical to other general tasks (for instance, image classification). An intuitive example would be the recently reported image denosing processor<sup>13</sup>, in which can be considered as a 4-f spatially filtering system (one can clearly observe a symmetry mask distribution for this DN with the frequency filter at the middle layer in that work). While the concept demonstrated here is in linear diffractive networks only, it has recently been reported that it is possible to perform nonlinear computing on such linear networks<sup>33-35</sup>. Therefore, it will certainly inspire further work on deciphering the mathematical meaning of complex networks with nonlinearities.

Overall, we have shown that diffractive optical networks can become physically interpretable while the physical meanings of diffractive surface per layer level have been unveiled after the training. This led to the first physically interpretable diffractive optical networks, as demonstrated here for consequently diffractive layers. We envision the extension of such physical interpretation to advanced tasks, then promoting interpretability of another crossover of optics and deep learning, such as nonlinear encoding<sup>35</sup>, recurrent linear scattering systems<sup>34</sup>, diffractive optical networks with nonlinear physical processes<sup>3,33</sup>, towards other wave-based learning approaches<sup>33</sup>, and finally, conventional deep learning in silico<sup>15</sup>, where only limited mathematical operations are investigated at this point.



## Materials and Methods

### Model training and numerical calculation

The diffractive networks are trained by adapting the wavefront matching approach<sup>17</sup>. Compared to typical deep learning algorithms, the wavefront matching algorithm reduces the degree of freedoms of the network by enforcing the phase smoothness<sup>36</sup>. In the training, each layer is defined as a complex value matrix with initial values of unitary. We applied the angular spectrum method to compute the free-space propagation of light and define the output mode correlation coefficient as the loss function. The masks are  $640 \times 640$  in size, with a pixel size of  $8 \mu\text{m} \times 8 \mu\text{m}$ . The wavelength of the input modes is 1550 nm. Other system parameters depend on the designed task and are listed in the following.

For the case of the vortex mode sorter with two masks (Fig. 2), we used LG modes with a beam waist parameter of  $400 \mu\text{m}$ . The interplane distance is set to be 20 mm, while the observation plane is 100 mm away from the last network surface. As mentioned in the main text, our dataset consists of 11 LG modes with  $l$  from -5 to 5, while  $l = 4, 2,$  and  $-2$  are included in the test set, and the rest are used as the training dataset. We used resultant fields from focused rectangle shapes of different phase gradients as the target output fields to train our DN starting from void masks. We noted that the choice of training set and test set (randomly) does not have observable effects on the results. The same trained masks are used in Fig. 5 to extrapolate the masks for different combinations of wavelengths and/or distances. The detection matrix is obtained following the approach in typical mode sorting work<sup>24</sup>.

For the case of the LG mode sorter with three masks (Fig. 3), LG modes with a beam waist parameter of  $170 \mu\text{m}$  are given as inputs. The interplane distances are 26.8 mm, while the observation plane is 50 mm away from the last network surface. Target resultant fields are Gaussian beams at the waist with a value of  $55 \mu\text{m}$ . The center-to-center distances for neighbor modes are set to be  $100 \mu\text{m}$ . Our dataset consists of 33  $\text{LG}_{l,p}$  modes with  $l$  from -5 to 5 and  $p$  from 0 to 2, while the cases  $\text{LG}_{-2,2}$ ,  $\text{LG}_{3,1}$ ,  $\text{LG}_{-3,1}$ ,  $\text{LG}_{4,0}$ ,  $\text{LG}_{1,0}$  are included in the test set, and the rest are used as the training dataset. We noted that the choice of training set and test set does not have observable effects on the results. Similar settings are applied for the LG mode sorter shown in Fig. 4, except for the total number of diffractive layers.

### Experimental setups

In our experiment, we used two cascaded multi-plane light conversion (MPLC) systems. Principles and illustrations of the MPLC system for generation and demultiplexing of modes can be found in other literatures<sup>17,37</sup>. Briefly, each MPLC system contains one spatial light modulator (Holoeye PLUTO-2.1, pixel number:  $1920 \times 1080$ , pixel size:  $8 \mu\text{m} \times 8 \mu\text{m}$ ), together with a reflective mirror. The light source (Keysight N7714A, wavelength: 1550 nm) we used has a beam waist of  $110 \mu\text{m}$ . The first MPLC generates high-quality LG modes with tunable beam waists and mode indices. For each LG mode, three sequential masks are trained and applied with the same protocol. The trained or numerical masks are applied in the second MPLC system and perform the sorting task. The detector (Hamamatsu, C12741-03, pixel number:  $640 \times 512$ , pixel size:  $20 \mu\text{m} \times 20 \mu\text{m}$ ) is placed at the output plane to capture the sorted mode intensity. The incident angle of the MPLC system is set to be 11 degree, which minimize the mode distortion.

## References

- 1 LeCun, Y., Bengio, Y. & Hinton, G. Deep learning. *Nature* **521**, 436-444 (2015).
- 2 Lin, X. *et al.* All-optical machine learning using diffractive deep neural networks. *Science* **361**, 1004-1008 (2018).
- 3 Yan, T. *et al.* Fourier-space diffractive deep neural network. *Physical Review Letters* **123**, 023901 (2019).
- 4 Kulce, O., Mengu, D., Rivenson, Y. & Ozcan, A. All-optical synthesis of an arbitrary linear transformation using diffractive surfaces. *Light: Science & Applications* **10**, 196 (2021).
- 5 Mengu, D., Rivenson, Y. & Ozcan, A. Scale-, shift-, and rotation-invariant diffractive optical networks. *ACS Photonics* **8**, 324-334 (2020).
- 6 Rahman, M. S. S., Li, J., Mengu, D., Rivenson, Y. & Ozcan, A. Ensemble learning of diffractive optical networks. *Light: Science & Applications* **10**, 14 (2021).
- 7 Lipton, Z. C. The mythos of model interpretability: In machine learning, the concept of interpretability is both important and slippery. *Queue* **16**, 31-57 (2018).
- 8 Ghorbani, A., Abid, A. & Zou, J. in *Proceedings of the AAAI Conference on Artificial Intelligence*. 3681-3688.
- 9 Towell, G. G. & Shavlik, J. W. Extracting refined rules from knowledge-based neural networks. *Machine Learning* **13**, 71-101 (1993).
- 10 Li, X. *et al.* Interpretable deep learning: Interpretation, interpretability, trustworthiness, and beyond. *Knowledge and Information Systems* **64**, 3197-3234 (2022).
- 11 Zhang, Y., Tiño, P., Leonardis, A. & Tang, K. A survey on neural network interpretability. *IEEE Transactions on Emerging Topics in Computational Intelligence* **5**, 726-742 (2021).
- 12 Wang, H. *et al.* Intelligent optoelectronic processor for orbital angular momentum spectrum measurement. *PhotonIX* **4**, 9 (2023).
- 13 Işıl, Ç. *et al.* All-optical image denoising using a diffractive visual processor. *Light: Science & Applications* **13**, 43 (2024).
- 14 McMahon, P. L. The physics of optical computing. *Nature Reviews Physics* **5**, 717-734 (2023).
- 15 Wright, L. G. *et al.* Deep physical neural networks trained with backpropagation. *Nature* **601**, 549-555 (2022).
- 16 Hughes, T. W., Williamson, I. A., Minkov, M. & Fan, S. Wave physics as an analog recurrent neural network. *Science Advances* **5**, eaay6946 (2019).
- 17 Fontaine, N. K. *et al.* Laguerre-Gaussian mode sorter. *Nature Communications* **10**, 1865 (2019).
- 18 Miller, D. A. All linear optical devices are mode converters. *Optics Express* **20**, 23985-23993 (2012).
- 19 Morizur, J.-F. *et al.* Programmable unitary spatial mode manipulation. *JOSA A* **27**, 2524-2531 (2010).
- 20 Wang, Q., Liu, J., Lyu, D. & Wang, J. Ultrahigh-fidelity spatial mode quantum gates in high-dimensional space by diffractive deep neural networks. *Light: Science & Applications* **13**, 10 (2024).
- 21 Allen, L., Beijersbergen, M. W., Spreeuw, R. & Woerdman, J. Orbital angular momentum of light and the transformation of Laguerre-Gaussian laser modes. *Physical Review A* **45**, 8185 (1992).
- 22 Shen, Y. *et al.* Optical vortices 30 years on: OAM manipulation from topological charge to multiple singularities. *Light: Science & Applications* **8**, 90 (2019).
- 23 Hossack, W., Darling, A. & Dahdouh, A. Coordinate transformations with multiple computer-generated optical elements. *Journal of Modern Optics* **34**, 1235-1250 (1987).
- 24 Berkhout, G. C., Lavery, M. P., Courtial, J., Beijersbergen, M. W. & Padgett, M. J. Efficient sorting of orbital angular momentum states of light. *Physical Review Letters* **105**, 153601 (2010).
- 25 Bryngdahl, O. Geometrical transformations in optics. *JOSA* **64**, 1092-1099 (1974).
- 26 Ruffato, G., Massari, M. & Romanato, F. Multiplication and division of the orbital angular

- momentum of light with diffractive transformation optics. *Light: Science & Applications* **8**, 113 (2019).
- 27 Zhou, Y. *et al.* Sorting photons by radial quantum number. *Physical Review Letters* **119**, 263602 (2017).
- 28 Prongué, D., Herzig, H.-P., Dändliker, R. & Gale, M. T. Optimized kinoform structures for highly efficient fan-out elements. *Applied Optics* **31**, 5706-5711 (1992).
- 29 Hochreiter, S. The vanishing gradient problem during learning recurrent neural nets and problem solutions. *International Journal of Uncertainty, Fuzziness and Knowledge-Based Systems* **6**, 107-116 (1998).
- 30 Ruffato, G., Rotunno, E., Giberti, L. & Grillo, V. Arbitrary conformal transformations of wave functions. *Physical Review Applied* **15**, 054028 (2021).
- 31 Kulce, O., Mengu, D., Rivenson, Y. & Ozcan, A. All-optical information-processing capacity of diffractive surfaces. *Light: Science & Applications* **10**, 25 (2021).
- 32 Goodman, J. W. *Introduction to Fourier optics*. (Roberts and Company publishers, 2005).
- 33 Li, Y., Li, J. & Ozcan, A. Nonlinear encoding in diffractive information processing using linear optical materials. *Light: Science & Applications* **13**, 173 (2024).
- 34 Yildirim, M., Dinc, N. U., Oguz, I., Psaltis, D. & Moser, C. Nonlinear processing with linear optics. *Nature Photonics*, 1-7 (2024).
- 35 Xia, F. *et al.* Nonlinear optical encoding enabled by recurrent linear scattering. *Nature Photonics*, 1-9 (2024).
- 36 Wu, L. Phase smoothing for diffractive deep neural networks. *Optics Communications* **556**, 130267 (2024).
- 37 Fang, J. *et al.* Optical orbital angular momentum multiplexing communication via inversely-designed multiphase plane light conversion. *Photonics Research* **10**, 2015-2023 (2022).